RSC Advances

PAPER

View Article Online
View Journal | View Issue

Cite this: *RSC Adv.*, 2024, **14**, 15491

Sono-responsive smart nanoliposomes for precise and rapid hemostasis application†

Qian Zhang,‡[a] Lichao Zhu,‡[b] Kaiyang Wang,*[b] Song Chen,[a] Yijiong Zhang,[a] Wei Song,[a] Long Qin,[a] Xijian Liu,[b] Yu Luo[b] and Jian Wan*[ab]

Massive hemorrhage caused by injuries and surgical procedures is a major challenge in emergency medical scenarios. Conventional means of hemostasis often fail to rapidly and efficiently control bleeding, especially in inaccessible locations. Herein, a type of smart nanoliposome with ultrasonic responsiveness, loaded with thrombin (thrombin@liposome, named TNL) was developed to serve as an efficient and rapid hemostatic agent. Firstly, the hydrophilic cavities of the liposomes were loaded onto the sono-sensitive agent protoporphyrin. Secondly, a singlet oxygen-sensitive chemical bond was connected with the hydrophobic and hydrophilic ends of liposomes in a chemical bond manner. Finally, based on the host guest effect between ultrasound and the sono-sensitizer, singlet oxygen is continuously generated, which breaks the hydrophobic and hydrophilic ends of liposome fragments, causing spatial collapse of the TNL structure, swiftly releases thrombin loaded in the hydrophilic capsule cavity, thereby achieving accurate and rapid local hemostasis (resulted in a reduction of approximately 67% in bleeding in the rat hemorrhage model). More importantly, after thorough assessments of biocompatibility and biodegradability, it has been confirmed that TNL possesses excellent biosafety, providing a new avenue for efficient and precise hemostasis.

Received 11th December 2023
Accepted 22nd April 2024

DOI: 10.1039/d3ra08445k

rsc.li/rsc-advances

Introduction

Thrombin, a multifunctional serine protease, is produced in cells upon injury. Its production during coagulation is crucial to the effective functioning of hemostasis.[1,2] Its main advantage lies in its powerful ability to catalyze the conversion of fibrinogen to fibrin, and it is a key accelerator in the process of blood coagulation.[3,4] However, the major challenge is to maintain the delicate equilibrium between the dosage of thrombin and its safety.[5,6] High concentrations may result in excessive coagulation, leading to thrombosis and serious complications.[7,8] Therefore, the thrombin should be safely controlled under specific conditions until it is triggered to be selectively released at the bleeding site for hemostatic purposes.

The emergence of nanotechnology has paved the way for an exciting new area in the creation of sophisticated materials for hemostasis. Nanomaterials offer unparalleled advantages in this critical biomedical application, including an increased surface-to-volume ratio of reactive surfaces,[9,10] customizable physical properties,[11,12] chemical properties,[13,14] and the potential for targeted drug delivery.[15–18] Various nanomaterials, such as metal nanoparticles, polymer nanofibers, and hybrid nanocomposites, have been developed to accelerate coagulation cascades and deliver procoagulants.[19–21] But unfortunately, many nanomaterials for hemostasis have issues regarding lack of the "smart" response mechanisms that are critical for adaptive and precise bleeding control.[22,23]

Sono-responsive nanoliposome are developed as smart nanomaterials, in which the nanoliposome can be activated to unload the carried drug by ultrasound (US). US is a form of mechanical sound wave with a notable capacity for deep tissue penetration of approximately 10 cm, thereby facilitating targeted therapeutic interventions for subcutaneous structures.[24] Ultrasonic waves could provide two advantages with the smart hemostasis nanomaterial, including non-thermal and thermal effects. On one hand, the activation of sono-sensitizer within the material by US can stimulate the generation of reactive oxygen species (ROS) that disrupt the ROS-sensitive bond within the physical matrix and cause the structure collapse to release the loaded drugs. On the other hand, the thermal effect arises from the absorption of US by biological tissues, which undergoes conversion into mechanical compression and subsequent generation of thermal energy.[25] This could

[a]*Department of Emergency and Critical Care Medicine, Shanghai Pudong New Area People's Hospital, No. 490 South Chuanhuan Road, Shanghai 201299, P. R. China. E-mail: wanjian@shpdph.com*

[b]*Shanghai Engineering Technology Research Center for Pharmaceutical Intelligent Equipment, Shanghai Frontiers Science Research Center for Druggability of Cardiovascular Noncoding RNA, Institute for Frontier Medical Technology, College of Chemistry and Chemical Engineering, Shanghai University of Engineering Science, No. 333 Longteng Road, Shanghai 201620, P. R. China. E-mail: kaiyang.wang@sues.edu.cn*

† Electronic supplementary information (ESI) available. See DOI: https://doi.org/10.1039/d3ra08445k

‡ These authors contributed equally to this paper as first author.

potentially help to close up the damaged vessels. Such specialized nanoliposome can combine nanoscale size and responsiveness to external US stimuli, providing a bilayer advantage. These nanoliposome can be loaded with thrombin and safely injected into the body without causing any adverse effects, additionally, they can be remotely activated by US for rapid and targeted hemostasis.[26–28] This provides a highly adjustable, efficient, and non-invasive method of bleeding control, in line with the clinical need for rapid and adaptive solutions.

Herein, a sono-responsive smart nanoliposome thrombin@liposome (TNL) as the next generation of hemostatic material was investigated in terms of properties, effectiveness, and potential clinical utility. Specifically, this research integrated the benefits of US's ability to penetrate deep tissues and the efficiency of thrombin in clotting to devise an advanced, safe, and highly effective collaborative technique for precise hemostasis. First, the hydrophilic cavities of the liposome was loaded onto protoporphyrin as a sono-sensitizer which produces singlet oxygen ($^1O_2$) upon sono-activation. Then the liposome was modified by employing a $^1O_2$-sensitive linker, to connect the hydrophilic and hydrophobic section of the liposome, to create the $^1O_2$-responsive liposome. The thrombin was then sealed inside these liposomes to make TNL. The TNL was introduced into the body through tail vein injection, and a US probe was aimed directly toward the location of hemorrhage to activate the TNL. Under the effect of US, the sono-sensitizer in the liposome generates $^1O_2$ to disconnect the hydrophilic and hydrophobic components of liposome, which ultimately causes the TNL framework to break down. On one hand, this facilitates the discharge of thrombin at the designated clot-forming locations, which elevates the local thrombin level, ensuring a swift hemostatic response. On the other hand, the thrombin-loaded liposome remain intact in other organs or tissues without being affected by exogenous US stimuli, ensuring that thrombin is still "captured" inside and avoiding the risk of embolism. This work combines a highly precise US probe to minimize the risk of off-target effects and ensure that activation of the TNL occurs only at the intended site. Additionally, the release of thrombin can only be triggered by the generation of $^1O_2$, which is strictly controlled by the focused US exposure, to mitigate the risks associated with the unintended release thrombin in undesired locations. The proposed TNL system could provide advantages in terms of precision and application in challenging bleeding scenarios where traditional methods are inadequate or impractical. Such TNL system could provide valuable insights for future hemostatic materials.

Results and discussion

The sono-activated thrombin nanoliposome TNL (thrombin@liposome) is based on DSPE liposome because of its well-documented biocompatibility and biosafety profiles. DSPE is commonly utilized in the development of biomaterials, particularly in drug delivery systems, making it an ideal candidate for *in vivo* applications. Another key factor of choosing DSPE is its stability of liposome and its prolonged circulation time in the bloodstream. TNL was prepared by membrane hydration. The liposome fragments of DSPE–PpIX, was prepared according to Scheme 1a and was confirmed by ^{1}H NMR (Fig. S1†). The DSPE-S–C$(CH_3)_2$–S-PEG$_{2k}$ was synthesised according to Scheme 1b, and then a film consisting of DSPE–PpIX, DPPC, and DSPE-S–C$(CH_3)_2$–S-PEG$_{2k}$ with a mass ratio of 5 : 1 : 25 was obtained by rotatory evaporation (Scheme 1c), in which DSPE-S–C$(CH_3)_2$–S-PEG$_{2k}$ serves as a $^1O_2$ sensitive fragment. The FT-IR confirms the inclusion of all the fragments within the final TNL (Fig. S2†). The thin film was then hydrated with ultra-pure water containing thrombin. Through hydrophilic interactions, thrombin was encapsulated into the $^1O_2$ sensitive liposome, and TNL was fabricated.

In a bleeding scenario, the TNL can be injected *via* intravenous injection. As shown in Scheme 1d, TNL was administrated to mice with tail vein injection, and a bleeding simulation was conducted by removing half of the liver lobe near the lesser curvature of the stomach. The bleeding site was then treated with US which provides a dual hemostasis effect: (a) the sono-sensitizer can produce $^1O_2$, which can lead to the disruption of the bonds between the hydrophilic and hydrophobic liposome. This results in the breakdown of the capsule structure and facilitates the release of the encapsulated thrombin, thereby hastening the hemostasis process. (b) The US can also generate heat and cause the blood within the vessels to clot, forming a thrombus. The thrombus can seal off the vascular openings, block bleeding points, and achieve hemostatic effects as well. Under the dual hemostasis effect from the TNL and US, a precise controlled release of thrombin at the required hemostatic sites, can elevate the local concentration of thrombin and achieve a rapid hemostasis.

Transmission electron microscopy (TEM) images showed that the TNL exhibited a spherical vesicle with a uniform size distribution (Fig. 1a and b). The hydrate particle size was determined by dynamic light scattering (DLS), the particle size of TNL was about 100 $\pm$ 6 nm (Fig. 1c) which was slightly larger than the observed size from the TEM. This was due to the DLS measures the hydrodynamic diameter of particles in suspension, which includes not only the core and lipid layer, but also the solvation layer. Additionally, TNL might slightly collapse or flatten on TEM grids during sample preparation due to dehydration, leading to an apparent smaller size compared to their native state in solution. Fig. 1d showed the TNL had a zeta potential of -24.1, indicates that the dispersed aqueous solution of TNL is not easy to coagulate. Additionally, the stability study of the TNL was conducted over 7 days, and the particle size maintained around 100 nm over the period (Fig. S3†).

To identify if the thrombin was successfully encapsulated in the liposome, UV-vis spectroscopy was conducted before and after loading the thrombin. The distinctive UV absorption peak observed at 280 nm is indicative of thrombin presence. Following the loading of thrombin into the liposome, this peak became visible in the absorption spectrum of the liposome (Fig. 1e). This demonstrates that thrombin was effectively encapsulated within the TNL.

Being a protein, alterations to thrombin's secondary structure during encapsulation could impinge on its biological enzyme function. To resolve this issue, circular dichroism

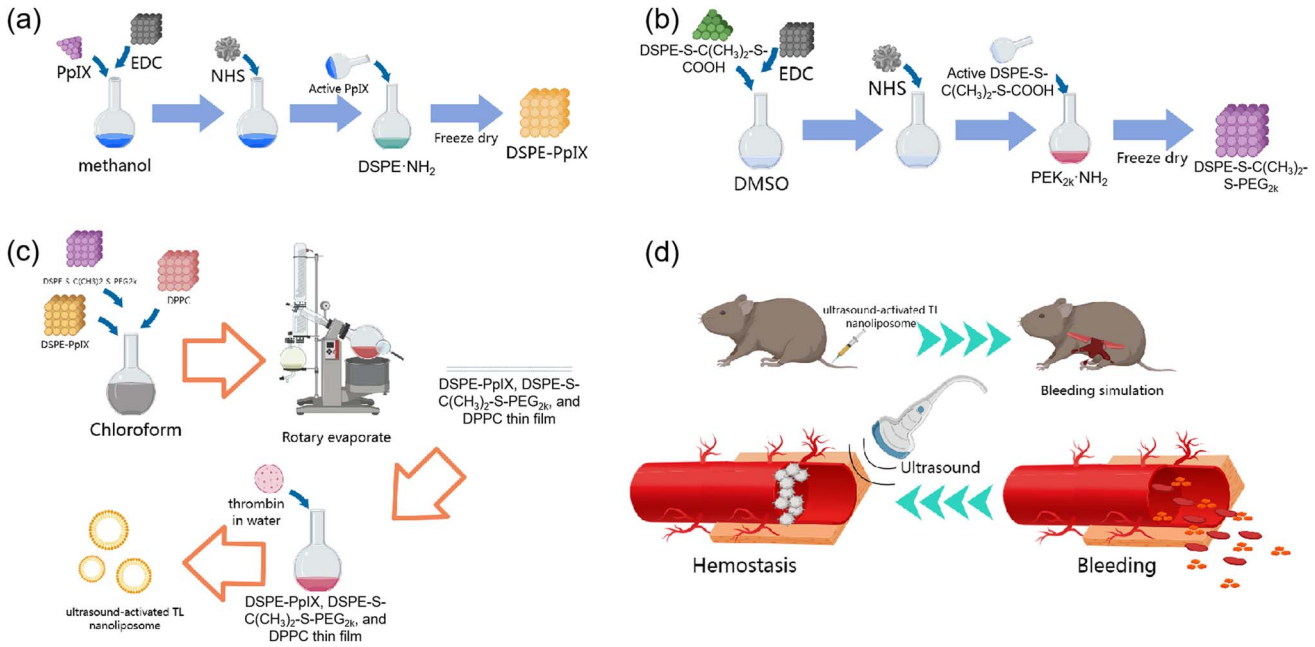

Scheme 1 Synthesis route of the liposome fragments of (a) DSPE–PpIX, (b) DSPE-S–C(CH_3)$_2$–S-PEG_{2k}, and (c) the TNL; (d) schematic illustration of the TNL after intravenous injection into the mouse. The TNL releases thrombin at the wound site to achieve hemostasis under US irradiation.

chromatography was conducted before and after loaded into the liposome. Fig. 1f showed that there were no changes in the thrombin's secondary structure, indicating the encapsulation process can preserve the thrombin's enzymatic activity.

Ultrasound-induced drug release performance

The TNL was designed to release thrombin from the disintegration of the liposome induced by the disruption of the $^1O_2$-sensitive linkers between the hydrophilic and hydrophobic ends. Under the US condition, the sonosensitizer within the liposome was able to generate $^1O_2$ to break the $^1O_2$-sensitive linker and release the encapsulated thrombin. $^1O_2$ has very short half life within the body (around 2.8 s).[32] Such rapid decay rate ensures that $^1O_2$ generated elsewhere, either through intrinsic biological processes or external sources, does not contribute to thrombin release. Thus, the system is primed for activation only when $^1O_2$ levels spike markedly due to the US treatment.

To verify if $^1O_2$ radicals can be generated under US conditions, the exact oxidative species generated were verified first with electron spin resonance (ESR) technique. As shown in Fig. 1g, under US conditions (1.0 W cm^{-2}, 5 min), a characteristic three equal height 1 : 1 : 1 triple signal confirms the generation of $^1O_2$ radicals from the liposome.

The released $^1O_2$ "cuts" the $^1O_2$-sensitive linker, causing the disintegration of the TNL capsule structure. As the liposome was disintegrated after the US treatment, an obvious destruction of the liposome was observed from the TEM imaging, as shown in Fig. 1h compared to Fig. 1a and b. Additionally, DLS measurements of the TNL also showed a reduction of 60% in size before and after the US treatment (Fig. S4†). This again confirmed that the liposome was sensitive to the US treatment and could be disintegrated efficiently. As a result, the thrombin contained in TNL was released. A UV-visible absorption detection was performed on the supernatant at different US times to investigate the releasing profile of thrombin. As shown in Fig. 1i, it was observed that thrombin can be released continuously within 5 min of US treatment.

In light of the aforementioned results, the operational mechanism of the liposome can be described as follows: with US stimulation, the protoporphyrin produces $^1O_2$, which breaks the $^1O_2$-sensitive bond in the liposome to releases thrombin on demand.

In vitro and *in vivo* biocompatibility evaluation

Prior to any biomedical use, it's essential to determine a material's biocompatibility. To assess cytotoxicity, a Cell-Counting Kit-8 (CCK-8) assay was performed. PC-001 cells were incubated with TNL for 24 h and 48 h. The outcomes indicated that the survival percentage of cells incubated with TNL exceeded 95% for 24 h (Fig. 2a) and remained above 90% for 48 h (Fig. 2b). When 200 g mL^{-1} of TNL was used, the 24 h and 48 h cell survival rates were still 90%, indicating that the TNL has good cellular compatibility. It should be emphasized that additional investigations into the long-term biocompatibility of TNL for *in vivo* applications are still necessary.

Therefore, the *in vivo* biocompatibility of the TNL was investigated next. Hemolytic test of TNL was firstly conducted with different amount of TNL, and the result showed that the TNL did not cause any hemolytic effect (Fig. S5†). The material was injected into the mice (20 mg kg^{-1}) and a long-term follow-up of the liposome with the TNL and NL (without thrombin) for

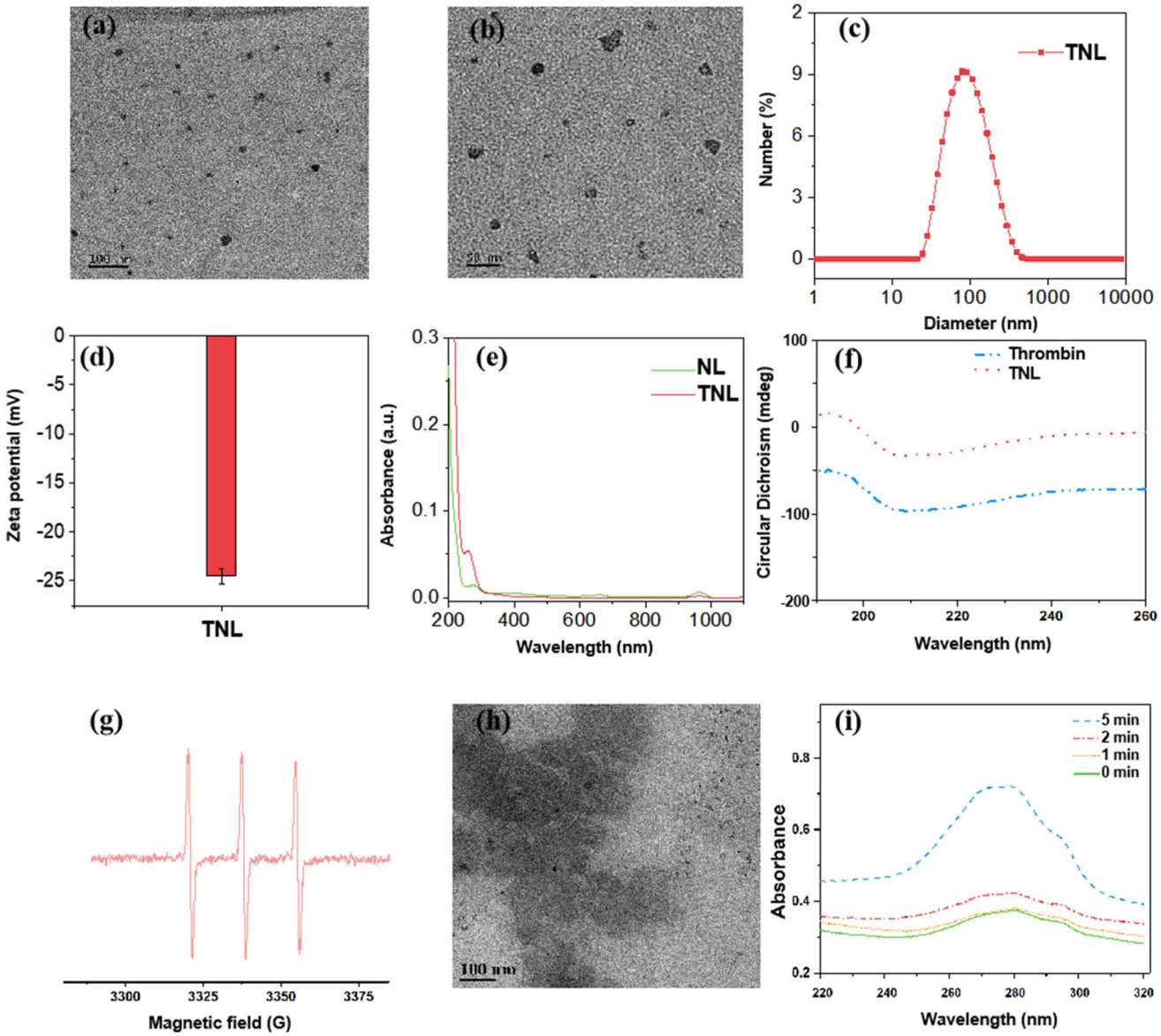

Fig. 1 Physical and chemical characterizations of the TNL: TEM images of the TNL (a) scale bar: 100 nm; and (b) scale bar: 50 nm; (c) particle size distribution; (d) zeta potential of the TNL; (e) UV-vis spectroscopy and (f) circular dichroic chromatography of the TNL before and after loading the thrombin; (g) ESR spectra of the TNL after ultrasonication (1.0 W cm^{-2}, 5 min); (h) TEM image of the TNL after the ultrasonic treatment; (i) UV-vis spectra of the release of thrombin after ultrasonication (1.0 W cm^{-2}), at different times.

90 days in mice model. Blood samples were collected every 30 days for routine blood tests. The results showed no significant variations in hemoglobin, hematocrit, platelet, red blood cells, and white blood cells when compared to the control group that received saline injections (Fig. 3a–e). The data affirmed that TNL did not elicit significant inflammatory or irregularities in the blood system. In addition, biochemical analyses were conducted to assess the potential impact of the TNL and NL on liver and kidney function. After 30, 60, and 90 days of the injection, no significant changes in BUN, creatinine, ALT, AST, and AKP levels were observed (Fig. 3f–h). These results emphasize that the TNL has good biocompatibility *in vivo* and does not impair important physiological functions. Integrating hematological and biochemical data, our experimental results supported that the TNL is a biocompatible material with long-term *in vivo* stability. It should be noted that these findings are consistent with the cytotoxicity assessments detailed in Fig. 2, corroborating the conclusion that TNL possesses a favorable safety profile for its potential use as an efficacious hemostatic agent.

Ultrasound hemostatic experiment

To examine the hemostatic performance of the liposome material, the simulations of bleeding were performed with saline solution and TNL. Before the simulation, each material was injected into the mice *via* the tail vein. Bleeding simulations were then performed on the mice. Specifically, a partial hepatectomy was performed on the liver lobe adjacent to the stomach's lesser curvature, as illustrated in Fig. 4a. After the creation

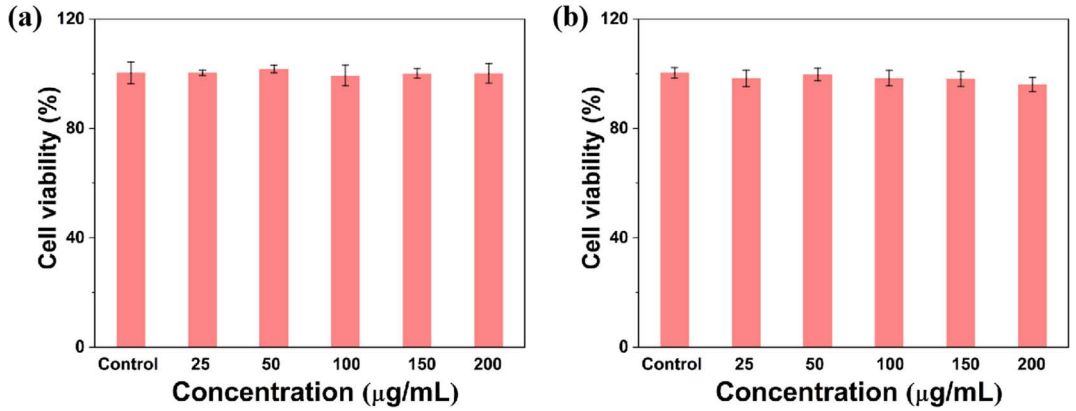

Fig. 2 CCK-8 results for the PC-001 cells after co-culture with the TNL for (a) 24 h and (b) 48 h.

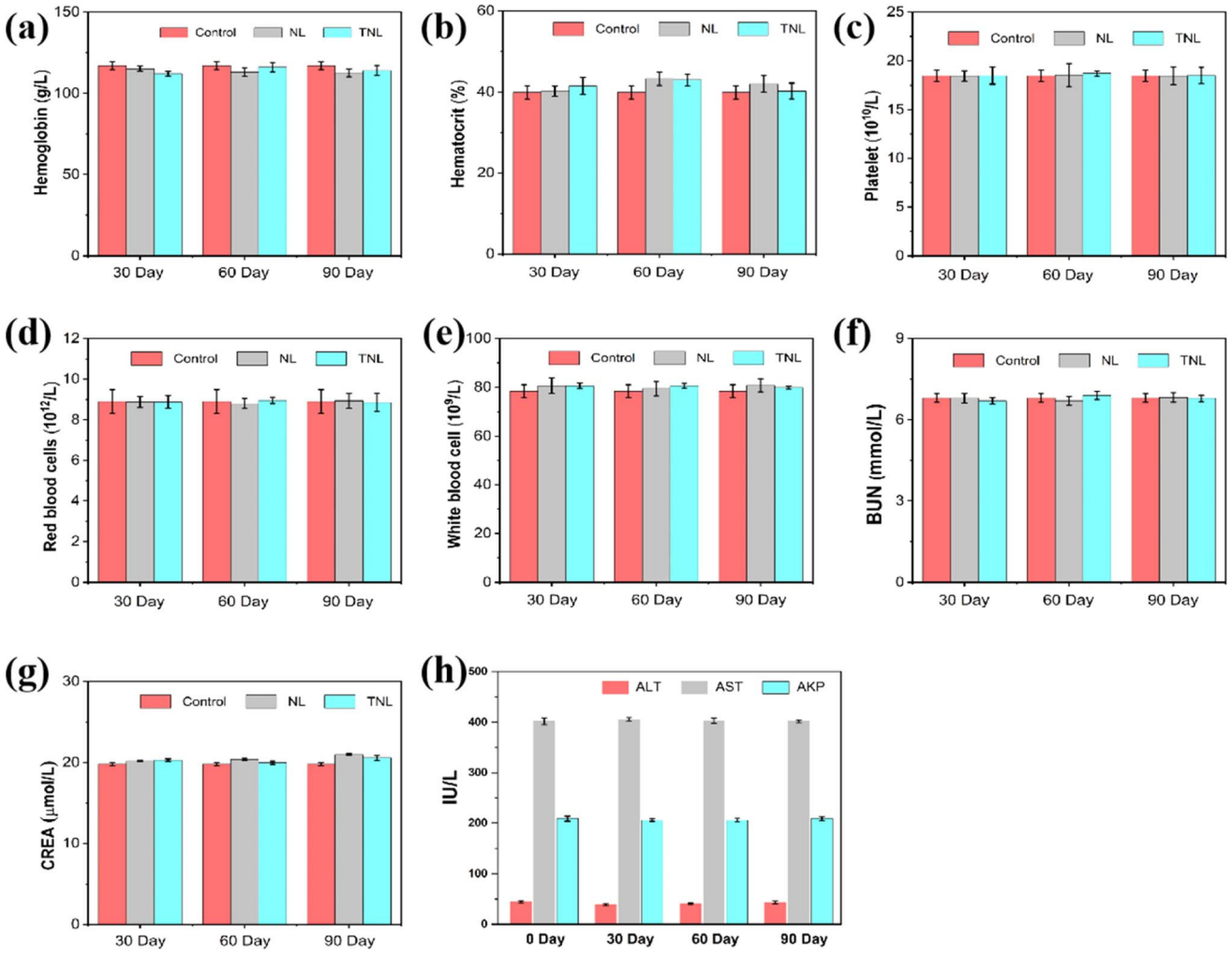

Fig. 3 Blood indexes of healthy mice after the injection of TNL and NL (without thrombin) (20 mg kg^{-1}, $n = 3$) at different time points: (a) hemoglobin, (b) hematocrit, (c) platelet, (d) red blood cells, and (e) white blood cell; kidney function indicators of healthy mice after injection of TNL and NL (20 mg kg^{-1}, $n = 3$) at different time points: (f) BUN, (g) CREA; (h) liver function indicators of healthy mice after injection of TNL.

of the bleeding site, filter paper was placed immediately below the cut to absorb the blood, similar to model described by Seon *et al.*[33] and Yang *et al.*[34] The wet filter paper weight was recorded to determine the total amount of bleeding and time to cease bleeding. An US probe was positioned over the injury with a separate piece of filter paper (Fig. 4b).

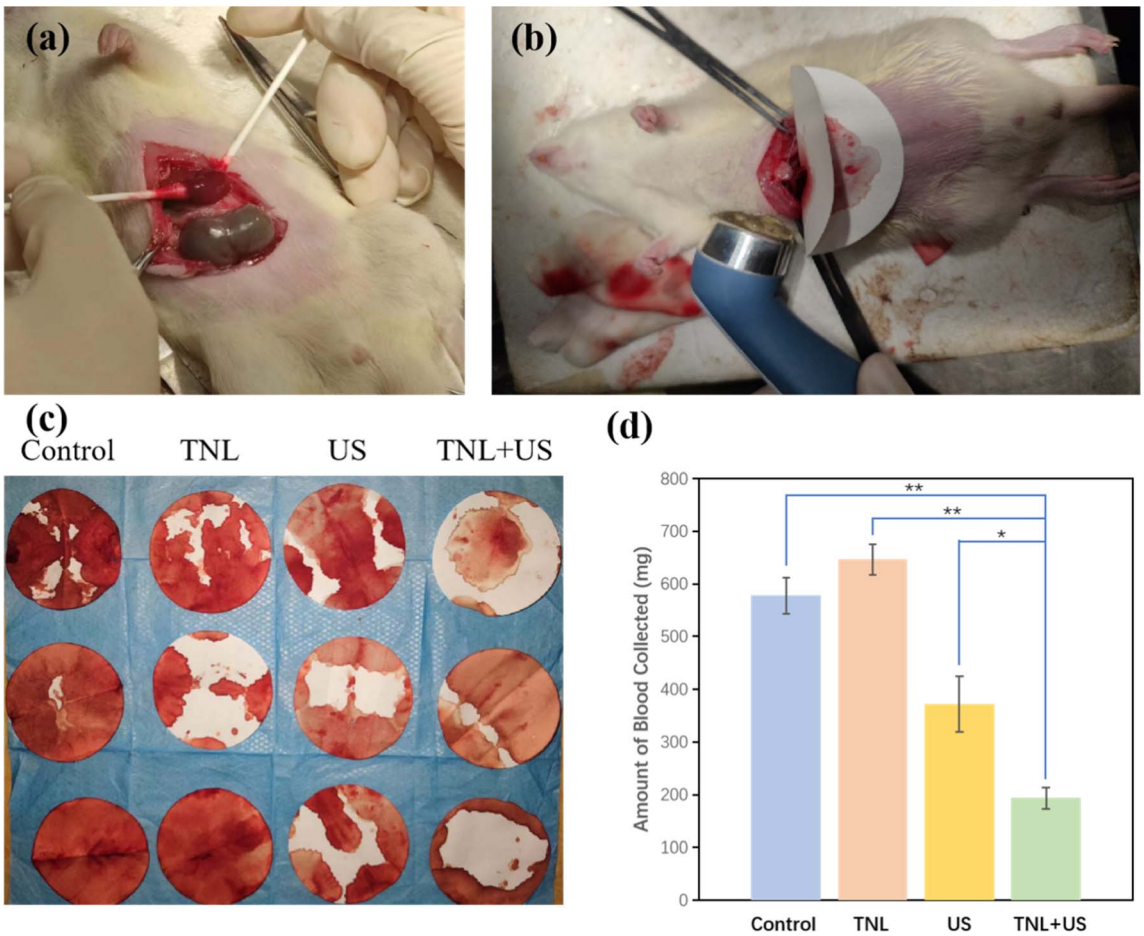

Fig. 4 (a) Demonstration of the bleeding simulation; (b) example of absorbing blood with a filter paper; (c) images of the filter paper with absorbed blood from different treatments; (d) quantitative data of blood collected on the filter paper ($n = 3$). Statistical analysis was performed by one-way ANOVA. *$P < 0.05$, **$P < 0.001$ and ***$P < 0.0001$.

The amount of the blood absorbed by the filter paper was recorded when hemostasis was achieved and the quantitative results were collected and summarized in Fig. 4c and d. Four groups (saline, TNL, US, and TNL + US) were assigned to evaluate the hemostasis efficiency. When TNL was solely used for hemostasis, there was no faster coagulation effect compared to the control group, around 600 mg of blood was lost before bleeding stopped for these two groups, indicating the TNL alone does not provide any hemostatic effects. Interestingly, during US-induced hemostasis, the amount of blood lost was about 65% of that in the control group, this was because the mechanical compression and subsequent heat generated by US could cause the blood within the vessels to clot and form a thrombus. The thrombus can seal off the vascular openings, block bleeding points, and achieve hemostatic effects. Outstandingly, for the TNL + US group, the wound blood loss was only 33% of that in the control group, and the blood loss was about 51% less than when US was used alone. The therapy with TNL + US group provided highly promising potential for *in vivo* hemostasis. Such significant reduction in the blood lost was resulted from the dual hemostasis effect: (a) the precise release of thrombin from the TNL at the bleeding site, and (b) the thrombus generated from the US.

When the mice were treated solely with normal saline or the TNL alone, there were no significant differences in wound hemostatic effect. After US treatment, the hemostatic effect was significantly improved, but the TNL + US treatment led to a more significant improvement in the hemostatic effect. This suggests that TNL can only be activated to release thrombin when US was applied. Such release of thrombin improves the local thrombin concentration around the sonicating area to achieve effective and precise hemostasis.

Conclusion

In summary, by using the membrane hydration method, a sono-responsive smart liposome TNL was successfully constructed and applied in hemostatic research. This study systematically assessed the performance and biocompatibility of the TNL as an innovative hemostatic material. The experimental results show that the TNL has good dispersity and stability, and thrombin can be efficiently loaded into the liposome. More importantly, the TNL can release thrombin rapidly under US thanks to the $^1O_2$-sensitive linker. The TNL also shows excellent *in vitro* and *in vivo* biocompatibility. By comparing the hemostasis effect

between normal saline, US, TNL, and TNL + US, the blood loss for the TNL + US group was only 33% of the control group. These findings not only confirm the great potential of TNL as an effective hemostatic material but also highlight its feasibility and safety in clinical applications. More importantly, compared to utilizing thrombin-based materials alone, the combination of US with hemostatic materials could provide a promising approach for efficient and precise hemostasis without the risk of causing blood clogs at unwanted sites.

Experimental

Materials and methods

Thrombin, *N*-hydroxysuccinimide, 1-ethyl-3-(3-dimethylaminopropyl)carbodiimide hydrochloride (EDC), and 1,2-dipalmitoyl-phosphatidylcholine (DPPC) were purchased from Sigma-Aldrich (Shanghai, China). Proto-porphyrin (PpIX), DSPE·NH_2, PEG_{2k}-NH_2, and $^1O_2$-cleavable fragment DSPE-S–$C(CH_3)_2$–S-COOH, and Cell Counting Kit-8 (CCK-8) were purchased from Aicheng Biotechnology Co., Ltd (Shanghai). Fetal bovine serum (FBS) was purchased from Gibco (New York, USA).

Synthesis of $^1O_2$-cleavable liposome fragments

Synthesis of DSPE–PpIX. Dissolving PpIX in 10 mL methanol to create a 0.3 mM solution. Next, swiftly mix EDC, at a concentration of 0.9 M in 1 mL methanol, into the PpIX solution and stir for 30 min. Following this, introduce NHS (0.9 M, dissolved in 1 mL methanol) to the mixture of PpIX and EDC, and continue stirring for an additional 3 h to activate the PpIX. Gradually add this activated PpIX to DSPE·NH_2 (with a concentration of 0.1 M in 10 mL methanol), stir continuously at 300 rpm for 72 h. The stoichiometry of the reactants was maintained at 3 : 1 molar ratio of PpIX : DSPE to achieve the formation of the monosubstituted product. To finalize the process, use a dialysis bag with a molecular weight cutoff of 5000 Da to purify the product in water. After dialysis, freeze-dry the substance and store it at 4 °C.

Synthesis of DSPE-S–$C(CH_3)_2$–S-PEG_{2k}. The method for creating DSPE-S–$C(CH_3)_2$–S-PEG_{2k} follows a similar protocol to that of DSPE–PpIX. Start by adding EDC (0.3 M, 1 mL DMSO) rapidly into the DSPE-S–$C(CH_3)_2$–S-COOH (0.1 M, 20 mL DMSO) solution and mix for 30 min. Next, introducing NHS (0.3 M in 1 mL DMSO) into the solution and mix thoroughly for an additional 3 h, which results in the activation of DSPE-S–$C(CH_3)_2$–S-COOH. This active intermediate was then slowly added into PEG_{2K}-NH_2 (0.1 M in 20 mL DMSO), ensuring constant stirring for 72 h. Finally, a 5000 Da dialysis bag was used to dialyze the product against water, and the purified product was freeze dried and stored at 4 °C.

Synthesis and characterization of the US activated TNL

Dissolving DSPE–PpIX, DPPC, and DSPE-S–$C(CH_3)_2$–S-PEG_{2k} in 10 mL chloroform with a mass ratio of 5 : 1 : 25. Rotary evaporation was then applied to remove the solvent. After that, thrombin in 20 mL of ultrapure water was added to the resultant film and stirred at room temperature for 1 h. A 0.22 μm PVDF syringe-driven filter (Millipore, Bedford, United States) and a 50 000 Da dialysis bag were used to filter and purify the final produced TNL (thrombin@liposome, named TNL) and stored at 4 °C before use.

TEM imaging for the TNL was conducted with JEM 2100F. Zetasizer Nano series was used to analyse the hydrate particle size and zeta potential of the obtained TNL. UV-visible spectroscopy was used to verify the encapsulation of the thrombin at absorption peak of 282 nm. Circular dichroism chromatography was used to characterize the secondary structural changes of thrombin before and after encapsulation.

Ultrasound-induced drug release performance

Electron spin resonance (ESR) spectra was used to detect singlet oxygen ($^1O_2$) generated from the TNL. The quantification of thrombin release was conducted utilizing UV-visible spectroscopy. In detail, 25 mg of TNL was dispersed in 25 mL of PBS buffer and subsequently placed into a 50 mL flat-bottomed centrifuge tube. The suspension was subjected to sonication over a range of 0 to 5 min with an intensity of 1 W cm^{-2}. Upon completion of the designated sonication period, the sample was centrifuged at a speed of 13 000 rpm for 10 min. The supernatant was then carefully extracted for analysis *via* UV-visible spectroscopy. The cumulative release of thrombin was determined by correlating the spectroscopic absorbance data to a standard curve derived from known concentrations of thrombin. Each measurement was replicated three times to ensure accuracy and reproducibility of the results.

Evaluation of hemolysis and cytotoxicity of the TNL

The hemolysis experiment follows the work of predecessors.[29–31] In this study, porcine pulmonary microvascular endothelial cells (PC-001) were utilized. The cells were cultured in DMEM supplemented with 10% fetal bovine serum (FBS), 100 U per mL penicillin, and 0.1 mg mL^{-1} streptomycin. This cell culture was maintained in a humidified incubator at a temperature of 37 °C and an atmosphere containing 5% CO_2. The endothelial cells were seeded in a 96-well plate at a density of 5000 cells per well and allowed to adhere for 12 h. Subsequently, TNL were introduced to the cells at varying concentrations (0, 10, 50, 100, 150, and 200 μg mL^{-1}), and the cells were co-incubated for an additional 24 and 48 h. Post-incubation, the cells were washed three times with PBS, after which CCK-8 assay reagent was added to each well. Following a further 2 h incubation period, cell viability was assessed by employing a microplate reader to measure the absorbance at a wavelength of 450 nm.

Evaluation of the *in vivo* biocompatibility of the TNL

The evaluation of TNL's long-term biocompatibility was conducted with healthy female Kunming mice, which were randomly separated into various groups. Mice in the TNL and NL (without thrombin) groups were administrated with the material at 20 mg kg^{-1} through the tail vein injection. Blood samples were collected from these mice at the initial point of the study (day 0) and subsequently at multiple time intervals following the injection (days 30, 60, 90) to perform a complete

blood and biochemical analysis, with each time point having three mice sampled ($n = 3$).

In vivo hemostatic performance evaluation of the TNL

All animal procedures were performed in accordance with the Guidelines for Care and Use of Laboratory Animals of Shanghai Pudong New Area People's Hospital and approved by the Medical Ethics Committee of Shanghai Pudong New Area People's Hospital (reference number: 2024-D-44). Mice were randomly divided into four groups ($n = 3$). Saline solution (1 mL) and TNL (material concentration 444 μg mL^{-1}, 1 mL) were administrated with tail vein injection. Wound simulations were then performed on the rats. Specifically, half of the liver lobe near the lesser curvature of the stomach was removed, and blood was absorbed using filter paper. The amount of blood absorbed by the filter paper was noted upon achieving hemostasis. For the groups involved with US, the US probe was placed on the wound (1 W cm^{-2}, 5 min, continuously).

Author contributions

QZ and LZ contribute equally in this work. Experimental design: QZ, LZ, KW, XL, YL, JW; experiments: QZ, LZ, KW, SC, YZ, WS, LQ; data analysis: QZ, LZ, KW, SC, YZ, WS, LQ, XL, YL, JW; manuscript writing: QZ, LZ, KW, XL, YL, JW.

Conflicts of interest

The authors declare no conflict of interest.

Acknowledgements

Jian Wan greatly acknowledge the financial support from the Project of Key Medical Discipline Group Construction in Shanghai Pudong New Area (No. PWZxq2022-13) and the Project of Clinical Outstanding Discipline Construction in Shanghai Pudong New Area (No. PWYgy2021-09).

References

1 O. M. Al-Amer, *Blood Coagulation Fibrinolysis*, 2022, **33**, 145–148.
2 S. R. Coughlin, *Nature*, 2000, **407**, 258–264.
3 M. Sun, M. H. Hao Pontius, S. Yang, T. Pendekanti, S. Raghunathan, J. A. Shavit and A. Sen Gupta, *J. Thromb. Haemostasis*, 2023, **21**, 983–994.
4 L. G. Mendes, F. V. Ferreira, M. S. Sielski, S. Livi, S. A. Rocco, M. L. Sforça, J. Burga-Sánchez, C. P. Vicente and L. H. I. Mei, *ACS Appl. Bio Mater.*, 2021, **4**, 5240–5250.
5 J. J. Posma, J. J. Posthuma and H. M. Spronk, *J. Thromb. Haemostasis*, 2016, **14**, 1908–1916.
6 J. B. Larsen and A. M. Hvas, *Semin. Thromb. Hemostasis*, 2021, **47**, 759–774.
7 R. De Caterina and S. Goto, *Vasc. Pharmacol.*, 2016, **81**, 1–14.
8 Q. D. Zhang, Q. Y. Duan, J. Tu and F. G. Wu, *Adv. Healthcare Mater.*, 2024, **13**, e2302209.
9 M. Aflori, *Nanomaterials*, 2021, **11**, 396.
10 Y. Patil-Sen, *Emerging Top. Life Sci.*, 2021, **5**, 169–176.
11 D. Lee, K. Huntoon, J. Lux, B. Y. S. Kim and W. Jiang, *Nat. Rev. Bioeng.*, 2023, **1**, 499–517.
12 M. Sajid, *Curr. Opin. Environ. Sci. Health*, 2022, **25**, 100319.
13 N. Baig, I. Kammakakam and W. Falath, *Mater. Adv.*, 2021, **2**, 1821–1871.
14 N. Joudeh and D. Linke, *J. Nanobiotechnol.*, 2022, **20**, 262.
15 M. J. Mitchell, M. M. Billingsley, R. M. Haley, M. E. Wechsler, N. A. Peppas and R. Langer, *Nat. Rev. Drug Discovery*, 2021, **20**, 101–124.
16 A. Shah, S. Aftab, J. Nisar, M. N. Ashiq and F. J. Iftikhar, *J. Drug Delivery Sci. Technol.*, 2021, **62**, 102426.
17 I. Santana, H. Wu, P. Hu and J. P. Giraldo, *Nat. Commun.*, 2020, **11**, 2045.
18 B. B. Mendes, J. Conniot, A. Avital, D. Yao, X. Jiang, X. Zhou, N. Sharf-Pauker, Y. Xiao, O. Adir, H. Liang, J. Shi, A. Schroeder and J. Conde, *Nat. Rev. Methods Primers*, 2022, **2**, 24.
19 J. Du, J. Wang, T. Xu, H. Yao, L. Yu and D. Huang, *Molecules*, 2023, **28**, 5264.
20 M. Wang, X. Huang, H. Zheng, Y. Tang, K. Zeng, L. Shao and L. Li, *J. Controlled Release*, 2021, **337**, 236–247.
21 Y. Tian, Z. Tian, Y. Dong, X. Wang and L. Zhan, *RSC Adv.*, 2021, **11**, 6958–6971.
22 Y. Yang, Y. Du, J. Zhang, H. Zhang and B. Guo, *Adv. Fiber Mater.*, 2022, **4**, 1027–1057.
23 C. Zhang, Q. Yang, X. Meng, H. Li, Z. Luo, L. Kai, J. Liang, S. Chen and F. Chen, *Adv. Sci.*, 2023, **10**, 2303418.
24 X. Song, L. Feng, C. Liang, K. Yang and Z. Liu, *Nano Lett.*, 2016, **16**, 6145–6153.
25 X. Qian, Y. Zheng and Y. Chen, *Adv. Mater.*, 2016, **28**, 8097–8129.
26 R. Catania, D. Onion, E. Russo, M. Zelzer, G. Mantovani, A. Huett and S. Stolnik, *RSC Adv.*, 2022, **12**, 16561–16569.
27 A. G. Athanassiadis, Z. Ma, N. Moreno-Gomez, K. Melde, E. Choi, R. Goyal and P. Fischer, *Chem. Rev.*, 2022, **122**, 5165–5208.
28 K. M. Aguilar-Pérez, J. I. Avilés-Castrillo, D. I. Medina, R. Parra-Saldivar and H. M. N. Iqbal, *Front. Bioeng. Biotechnol.*, 2020, **8**, 579536.
29 Y. Fan, L. Liu, F. Li, H. Zhou, Y. Ye, C. Yuan, H. Shan, W. Zang, Y. Luo and S. Yan, *Front. Bioeng. Biotechnol.*, 2022, **10**, 923365.
30 K. Liang, Z. Li, Y. Luo, Q. Zhang, F. Yin, L. Xu, H. Chen and H. Wang, *Small*, 2020, **16**, 1906985.
31 Z. Yang, Y. Luo, Y. Hu, K. Liang, G. He, Q. Chen, Q. Wang and H. Chen, *Adv. Funct. Mater.*, 2021, **31**, 2007991.
32 K.-K. Wang, S. Song, S.-J. Jung, J.-W. Hwang, M.-G. Kim, J.-H. Kim, J. Sung, J.-K. Lee and Y.-R. Kim, *Phys. Chem. Chem. Phys.*, 2020, **22**, 21664–21671.
33 G. M. Seon, M. H. Lee, B.-J. Kwon, M. S. Kim, M.-A. Koo, D. Kim, Y. Seomun, J.-T. Kim and J.-C. Park, *Acta Biomater.*, 2017, **48**, 175–185.
34 X. Yang, W. Liu, Y. Shi, G. Xi, M. Wang, B. Liang, Y. Feng, X. Ren and C. Shi, *Acta Biomater.*, 2019, **99**, 220–235.